Cobalt-Exchanged Poly(Heptazine Imides) as Transition Metal–N_x Electrocatalysts for the Oxygen Evolution Reaction

*Meng-Yang Ye, Shuang Li, Xiaojia Zhao, Nadezda V. Tarakina, Christian Teutloff, Wing Ying Chow, Robert Bittl, and Arne Thomas**

Poly(heptazine imides) hosting cobalt ions as countercations are presented as promising electrocatalysts for the oxygen evolution reaction (OER). A facile mixed-salt melt-assisted condensation is developed to prepare such cobalt poly(heptazine imides) (PHI-Co). The Co ions can be introduced in well-controlled amounts using this method, and are shown to be atomically dispersed within the imide-linked heptazine matrix. When applied to electrocatalytic OER, PHI-Co shows a remarkable activity with an overpotential of 324 mV and Tafel slope of 44 mV dec^{-1} in 1 M KOH.

Water splitting is a sustainable and low-cost method to gain clean energy.[1–3] In this process, the oxygen evolution reaction (OER) is the more challenging half-reaction, due to its slow kinetics, which stems from a four-electron oxidation process. Indeed, the slow progress in optimizing this half-reaction has largely hindered the development of overall water splitting devices.[4–6] In addition, the so far best-performing OER catalysts are based on noble metals (e.g., Ir and Ru),[7–9] for which the high cost and scarcity limit their utilization especially in large-scale applications.[5,10,11] Hence, the exploration of high-performance noble-metal-free electrocatalysts for OER has become one of the major challenges in the field of electrocatalysis.

Carbon materials featuring transition metal–N_x sites have recently been shown to be active in various electrocatalytic reactions.[12–14] It was reported that in these materials, metal species interact synergistically with nitrogen atoms to modify the local electronic structure of the catalyst and consequently optimize the surface adsorption of intermediates.[15,16] Therefore, the activity of transition metal–N_x catalysts is often comparable to noble metal catalysts in various electrocatalytic reactions.[12–16] Consequently, the design of electrocatalysts with abundant and well-dispersed metal–N_x active sites is a promising approach toward high-performance noble-metal-free electrocatalysts. However, in such metal–N_x–C systems, the amount, dispersion, and type of the nitrogen dopant in the carbon matrix is relatively difficult to identify and control.[17]

In this respect, carbon nitrides are intriguing candidates as supporting materials for transition metal–N_x catalysts, as their abundant and structurally defined nitrogens provide a high amount of coupling sites.[18,19] However, because of the relatively low conductivity and electrochemical stability of carbon nitrides, for electrocatalytic applications these materials have to be mostly mixed with carbon materials.[20] Indeed the few attempts to apply metal-doped carbon nitrides directly for photoelectro- or electrocatalysis have not yet obtained competitive activities.[21]

Poly(heptazine imide) (PHI) is a new member of the carbon nitride family.[22,23] Unlike polymeric carbon nitride condensed by heating, e.g., urea or cyanamide,[18,24–26] PHI is prepared by salt-melt-assisted condensation of more acidic precursors, such as triazole or tetrazole.[22,27] While in the former heptazine units are connected by amine bridges, in PHI the heptazine units are linked by deprotonated imides, whose charge is counterbalanced by metal cations introduced by the salt template.[22] The negatively charged nitrogen sites not only remarkably enhance the conductivity of the material, but also efficiently host various metals as countercations, yielding an excellent dispersion and periodicity within the structure.[23,27–30] Furthermore, PHI can host different metal ions in its structure, introduced during PHI formation or via post modification, i.e., ion exchange,[23,27,28] and is therefore a promising material for developing novel transition metal–N_x catalysts.

In this work, cobalt poly(heptazine imides) (PHI-Co) were synthesized based on a reported method,[28] with a Co salt ($CoCl_2$) additionally introduced to the eutectic KCl–LiCl melt

M. Y. Ye, Dr. S. Li, Dr. X. J. Zhao, Prof. A. Thomas
Department of Chemistry
Functional Materials
Technische Universität Berlin
Hardenbergstr. 40, 10623 Berlin, Germany
E-mail: arne.thomas@tu-berlin.de
Dr. N. V. Tarakina
Max Planck Institute of Colloids & Interfaces
Department of Colloid Chemistry
D-14476 Potsdam, Germany
Dr. C. Teutloff, Prof. R. Bittl
Freie Universität Berlin
Fachbereich Physik
Berlin Joint EPR Lab
Arnimallee 14, D-14195 Berlin, Germany
Dr. W. Y. Chow
Leibniz-Forschungsinstitut für Molekulare Pharmakologie im Forschungsverbund Berlin e.V. (FMP)
Campus Berlin-Buch
Robert-Rössle-Str. 10, 13125 Berlin, Germany
The ORCID identification number(s) for the author(s) of this article can be found under https://doi.org/10.1002/adma.201903942.

DOI: 10.1002/adma.201903942

Table 1. Amount of cobalt in PHI-Co and corresponding weight percentage of $CoCl_2$ used in the salt template.

Samples	Cobalt in samples [wt%]	$CoCl_2$ in salt template [wt%]
PHI	0	0
PHI-Co-0.2	0.17	0.5
PHI-Co-0.5	0.45	1
PHI-Co-0.8	0.83	2
PHI-Co-1.4	1.43	3
PHI-Co-2.6	2.61	5
CN-Co	0.52	–

during PHI preparation. Various amounts of cobalt ions can be intercalated into the PHI structure using this method, without causing structural rearrangement as was observed when an ion-exchange method is applied.[27] The PHI-Co electrocatalyst shows enhanced OER activity compared to a cobalt-doped polymeric carbon nitride with an overpotential of 324 mV in 1 M KOH, well comparable to state-of-the-art OER electrocatalysts under similar conditions.[31,34]

In a typical PHI preparation, the precursor 5-aminotetrazole was first mixed with an eutectic KCl–LiCl mixture. The mixture was then heated in argon flow at 550 °C for 8 h to obtain the yellowish-brown PHI. To introduce cobalt ions into the PHI structure, different amounts of $CoCl_2$ (0.5–5 wt%) were added to the KCl–LiCl mixture and then 5-aminotetrazole was added. These mixtures were as well heated in argon at 550 °C for 8 h to obtain greenish-brown PHI-Co (for the detailed synthesis protocol, see the Supporting Information).

The content of cobalt in the as-prepared PHI-Co's was evaluated by inductively coupled plasma optical emission spectrometry (**Table 1**) and varied from 0.17 to 2.61 wt%, when 0.5–5.0 wt% of $CoCl_2$ was added to the eutectic KCl/LiCl mixture. As the cobalt content in PHI-Co's increases proportionally with respect to the $CoCl_2$ amount in the salt template, it can be concluded that the amount of Co ions can be varied continuously using this method. As expected, the potassium amount within the PHIs is decreasing with increasing Co content (Table S1, Supporting Information), suggesting that the cobalt ions are partially replacing the potassium ions in the PHI structure. However, especially for samples with higher cobalt content, more Co^{2+} ions are introduced in PHI than K^+ ions are removed from the system. In PHI-K, not all bridging nitrogen sites are counterbalanced by K^+, as there are still considerable amounts of protons left in the structure. Therefore, it is not prerequisite that K^+ is replaced stoichiometrically by Co^{2+}, but Co can also occupy newly formed imide sites during synthesis, which seems to be particular the case at higher Co content. X-ray photoelectron spectroscopy (XPS) measurements were conducted to detect Li and Cl within the materials (Figure S1, Supporting Information). However, no contribution of these elements could be observed, indicating that Li has not been intercalated in the PHI structure and the salt template could be completely removed. If not noted otherwise, the PHI-Co described below refers to PHI-Co-0.5, which contains 0.45 wt% cobalt.

X-ray powder diffraction (XRD) measurements of the PHI-Co samples with different cobalt content and the cobalt-free potassium poly(heptazine) imide (PHI) were carried out (**Figure 1** and Figure S2, Supporting Information). In the XRD pattern of PHI, the diffraction peak at 8° can be ascribed to the periodicity of heptazine units within the layers while the diffraction peak at 27° corresponds to interplanar stacking of the layers.[22] Both peaks can also be observed in all PHI-Co samples, showing that the structure of poly(heptazine) imide backbone is well preserved in PHI-Co, despite the intercalated ions are partially changed from K^+ to Co^{2+}.

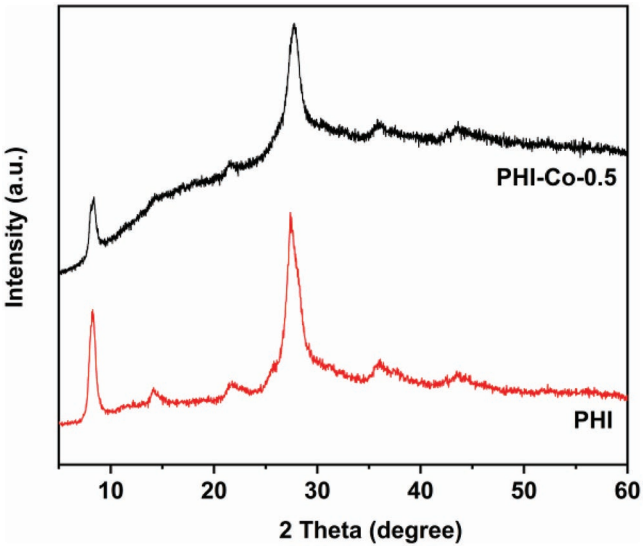

Figure 1. XRD patterns of PHI-Co-0.5 and PHI.

The chemical structure of PHI-Co is schematically shown in **Figure 2**a. XPS (Figure 2b–d), solid-state nuclear magnetic resonance (NMR) spectroscopy (Figure S3, Supporting Information), Fourier transform infrared (FT-IR) spectroscopy (Figure 2e), and electron paramagnetic resonance (EPR) (Figure 2f and Figure S4, Supporting Information) measurements of PHI-Co were compared with PHI. As observed in Figure 2b, the doublet peak in the XPS Co 2p spectrum centered at 780.4 eV with strong satellite features at 785.4 eV indicates cobalt in an oxidation state of Co(II) in the material. At the same time, no contribution of cobalt oxide can be observed in the O 1s spectrum of PHI-Co, nor any hint of $CoCl_2$ remaining in the sample (Figures S1 and S5, Supporting Information). Thus, it can be concluded that the cobalt in PHI-Co is mainly bound within the structure as counterion to the anionic imide sites of the PHI.[32] In the N 1s and C 1s XPS spectra (Figure 2c,d), PHI-Co shows very similar nitrogen and carbon species as PHI, indicating that the intercalation of cobalt has not changed the original structure of PHI. The peaks at 398.5 and 400.9 eV in the PHI-Co N 1s spectrum can be addressed to the C−N=C (ring N in heptazine unit), $N-C_3$ (central N in heptazine unit), while the contribution at 399.6 eV corresponds to the NH_x groups. The major contribution in the C 1s spectrum at 288.1 eV can be assigned to N−C=N in the heptazine unit.[33] A small peak shift and change in intensity between PHI-Co and PHI indicate a slight change of condensation degree when cobalt is present. Additionally, the peaks in the C 1s spectrum at 284.8 and 286.4 eV can be attributed to adventitious carbon and hydroxylated surface carbon atoms, respectively.[32] The other small

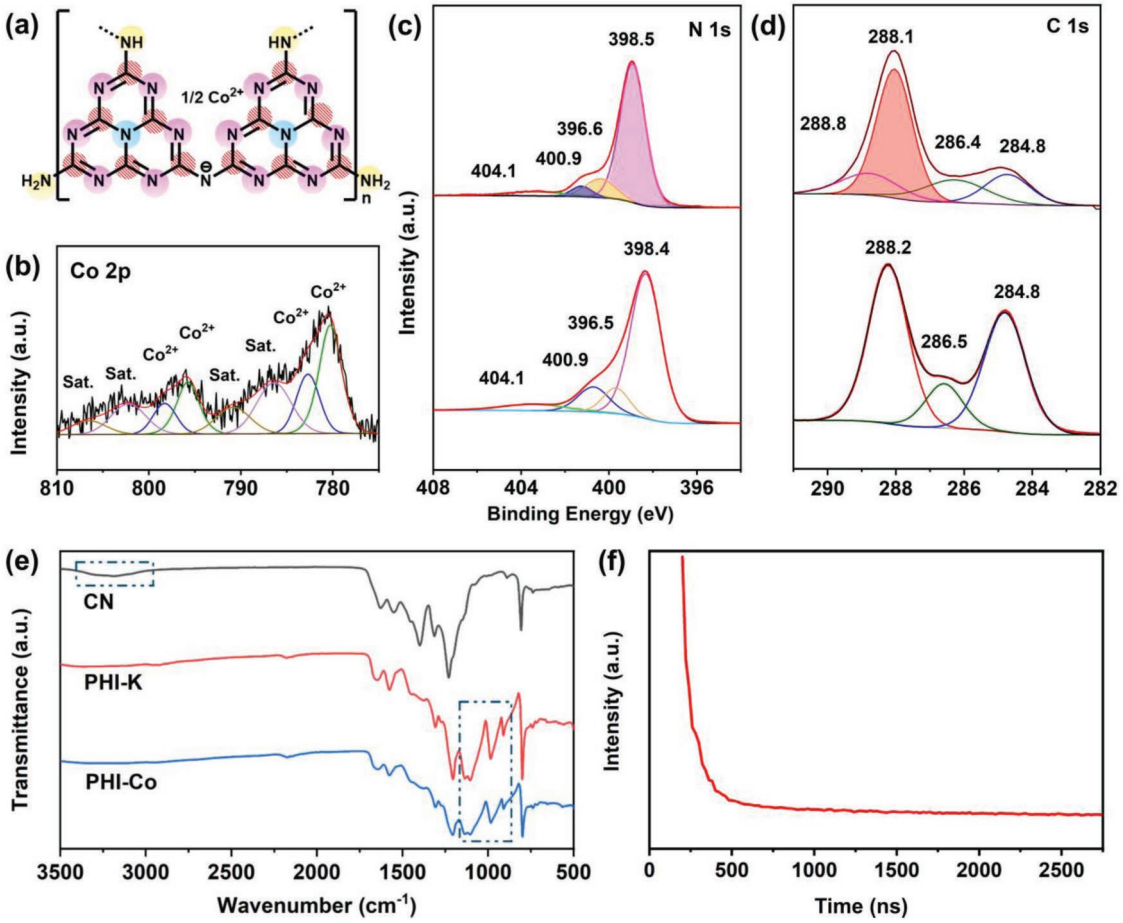

Figure 2. a) Chemical structure of PHI-Co. b) Co 2p XPS spectra of PHI-Co. c,d) N 1s and C 1s XPS spectra of PHI-Co and PHI, respectively. e) FT-IR spectra of polymeric CN, PHI, and PHI-Co, respectively. f) 2-Pulse ESEEM of PHI-Co at 5 K and a field position of $B = 310$ mT, pulse sequence: $\pi/2$–τ–π with pulse length $\pi = 16$ ns, and pulse separation $\tau = 200$ ns, τ increment = 20 ns, shot repetition time 0.5 ms, 400 averages.

peaks appeared in the C 1s spectra at 288.8 eV and in the N 1s spectra at 404.1 eV are due to surface oxidation.[27,32,35] The similar IR and NMR spectra of PHI-Co and PHI (Figure 2e and Figure S3, Supporting Information) further prove that they share a very similar chemical structure.[28] Moreover, when comparing the IR spectra with polymeric carbon nitride (CN), first the vibration of NH_x groups decreases in both PHI and PHI-Co, while several new peaks emerge in the range of 865–1158 cm^{-1}, due to the intercalation of metal ions.[28] Pulse EPR spectroscopy at 9.7 GHz (X band) and 5 K yields a 300 mT broad field swept echo spectrum of the Co^{2+} (Figure S4a, Supporting Information), which can be assigned to Co^{2+} in S = 3/2 state.[36] To investigate a specific binding between the Co^{2+} and PHI, electron spin echo envelope modulation (ESEEM) spectroscopy was performed at the peak position (310 mT) of the EPR spectrum. The echo decay with increasing pulse separation τ in a 2-pulse $\pi/2$–τ–echo sequence is monotonous without any detectable modulation effect (Figure 2f), which can be corroborated by a 2D stimulated echo $\pi/2$–τ–$\pi/2$–T–$\pi/2$–echo experiment. The 2D Fourier transform shows no resolved modulation signatures beyond the noise level (Figure S4b, Supporting Information). This lack of any resolved hyperfine interaction between the Co and PHI structure indicates that no specific Co-N ligand is formed.

The morphology of PHI-Co was observed via scanning electron microscopy (SEM) and annular dark-field scanning transmission electron microscopy (ADF-STEM). The SEM images (Figure S6, Supporting Information) show that PHI-Co possess a very similar morphology to PHI. In ADF-STEM, the presence of cobalt in PHI-Co can be easily spotted (**Figure 3**). The low magnification ADF-STEM images of PHI-Co (Figure 3a,b) show uniform brightness, indicating that cobalt in the PHI structure does not aggregate to form cobalt nanoparticles. The homogenous distribution of cobalt ions can be further confirmed by elemental mapping (Figure 3, inset), where the signal of cobalt can be detected over the entire measured part of the sample. High-resolution (HR) ADF-STEM images of PHI-Co (Figure 3c) show bright dots of cobalt ions dispersed in the darker PHI matrix, confirming that Co in PHI structure is dispersed atomically.

The electrocatalytic performance of PHI-Co with different cobalt contents was evaluated in 1 M KOH solutions, with a mass loading of 0.38 mg cm^{-2} on glassy carbon rotating disk electrodes and compared with pure Co, pure PHI, a mechanical mixture of PHI and 0.45 wt% Co (PHI+Co), carbon nitride (CN), cobalt-doped carbon nitride (CN-Co), and a commercial Ir/C catalyst. All the aforementioned electrodes were prepared in the

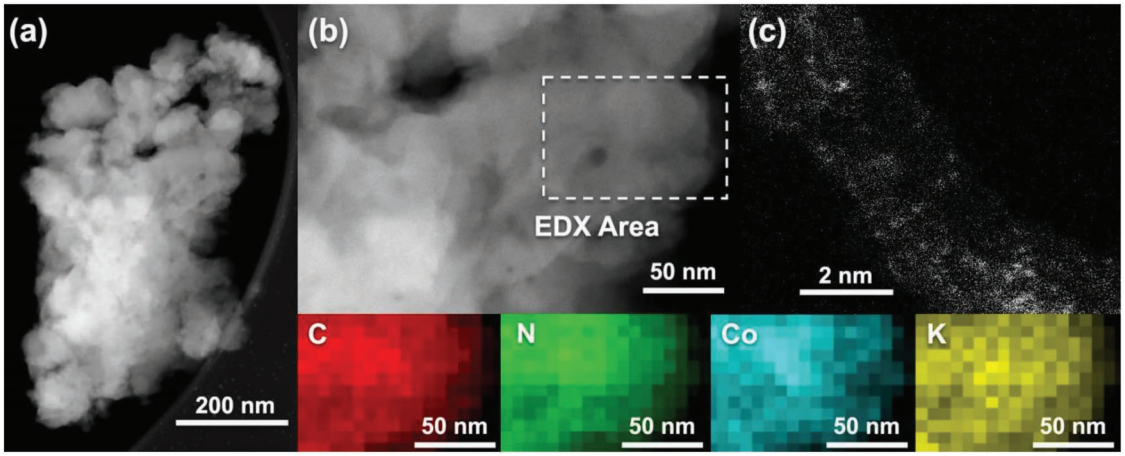

Figure 3. a) ADF-STEM image of a typical PHI-Co agglomerate. b) Enlargement from (a) with energy dispersive X-ray (EDX) elemental maps of C, N, Co, K elements shown at the bottom. The solid white rectangle indicates the area from which EDX maps were obtained. c) HR ADF-STEM image of PHI-Co, bright spots represent cobalt atoms.

same manner. The OER activities of these catalysts were evaluated by polarization curves (**Figure 4**a), corresponding Tafel plots were extracted from the polarization curves to calculate the Tafel slopes and exchange current densities (Figure S7a and Table S2, Supporting Information). The electrochemically active surface area of different PHI-Co's was compared by calculating the double layer capacitance (C_{dl}) of the PHI-Co samples (Figure S8a–g and Table S2, Supporting Information). Mass activities per mg cobalt were also calculated to normalize the activities of cobalt-containing samples (Figure S8h, Supporting Information). As depicted in Figure 4a, PHI-Co's show significantly enhanced OER activity compared to Co and pure PHI, while they are also obviously more active than a physical mixture of PHI and Co (PHI+Co) or a cobalt-doped polymeric carbon nitride (CN-Co) with similar Co content. This indicates that the atomic distribution of cobalt confined within the PHI structure leads to the

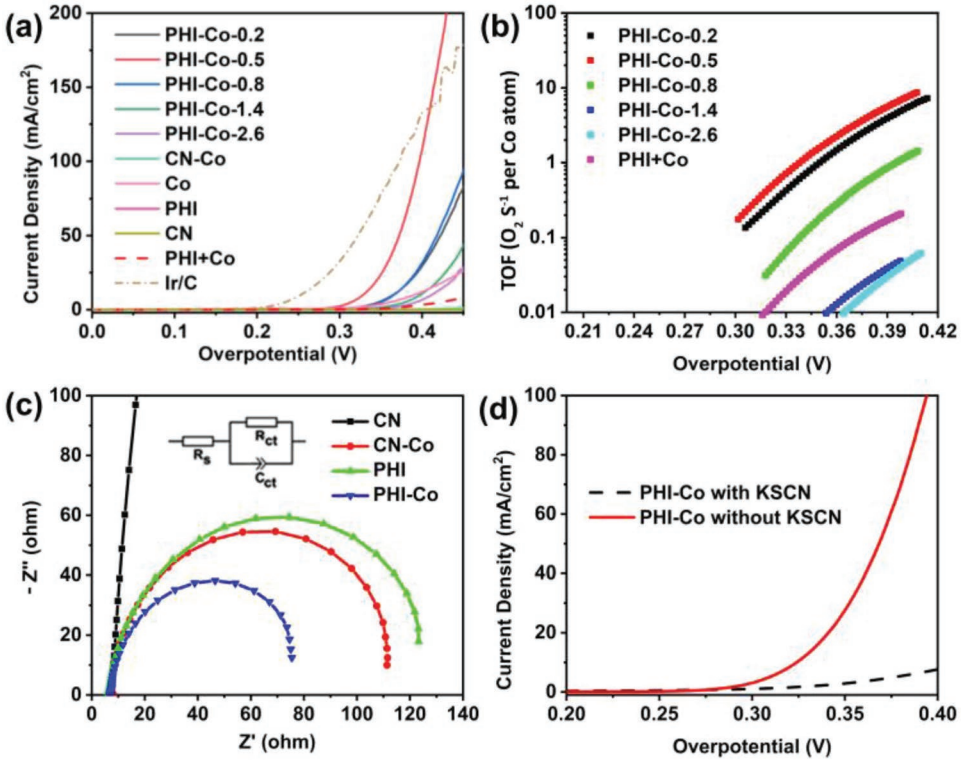

Figure 4. a) OER polarization curves of PHI-Co's, CN-Co, PHI, CN, Co, and PHI+Co. b) Corresponding turnover frequency to overpotential plots of PHI-Co's. c) Nyquist plots of PHI-Co, PHI, CN-Co, CN in 1 M KOH electrolyte, measured under the static potential of 1.6 V versus RHE, and the corresponding equivalent circuit (inset). d) OER polarization curves of PHI-Co-0.5 in 1 M KOH electrolyte before and after the addition of 10×10^3 M KSCN.

high OER activity. Among the PHI-Co's, PHI-Co-0.5 exhibit the lowest overpotential as well as the highest mass activity. Notably, PHI-Co-0.5 shows a very low overpotential (j = 10 mA cm^{-2}) of 0.324 V in N_2-saturated electrolyte (0.336 V in O_2-saturated electrolyte, Figure S7b, Supporting Information), which is a promising value when compared with other metal-doped polymer-based electrocatalysts. Moreover, despite the relative low conductivity due to its organic semiconducting nature,[22] PHI-Co-0.5 possess a competitive activity compared to some state-of-art carbon-based electrocatalysts (Tables S3-1 and S3-2, Supporting Information).[37–46] PHI-Co-0.5 shows both the largest exchange current density and the smallest Tafel slope among the PHI-Co's, which together lead to the fastest kinetics (Table S2, Supporting Information). All PHI-Co's have Tafel slopes in the range of 44–63 mV dec^{-1} (Table S2, Supporting Information), which is similar to other Co-containing catalysts.[47,48] The activity of PHI-Co's was further investigated by calculating the turnover frequency (TOF) of the electrocatalysts, with all the cobalt ions exposed on the surface considered as active sites. The TOF values were plotted against the applied overpotential (Figure 4b). Again, the TOF of PHI-Co-0.5 is superior to the other PHI-Co's and also the mechanical PHI+Co mixture at various overpotentials, that is PHI-Co-0.5 shows the highest activity per active site.

To get further insight into the kinetics of the OER process, electrochemical impedance spectra were recorded to yield the charge transfer resistances at 1.6 V versus reversible hydrogen electrode (RHE). In a Nyquist plot, the diameter and phase angle of the semicircle at high frequency stand for the charge transfer resistance (R_{ct}) and capacity (C_{ct}) at the interface of the catalyst and electrolyte, respectively, while the Z' axis intercept shows the resistance (R_s) relating to charge transport in the circuit.[20] As observed in the Nyquist plots (Figure 4c), the diameter of the semicircle (R_{ct}) is lowest for PHI-Co (84 Ω), compared with CN-Co (100 Ω), PHI (105 Ω), and CN (409 Ω), pointing to a sufficient charge transfer ability at the interface of the catalyst and electrolyte. To verify that Co^{2+} ions are responsible for the OER performance, a poisoning experiment was carried out by injecting 10×10^3 M KSCN (Figure 4d), which is known to poison metal-centered catalytic sites.[49] As seen in Figure 4d, the addition of SCN^- to PHI-Co-catalyzed OER indeed causes a remarkable increase of overpotential (j = 10 mA cm^{-2}) of more than 0.1 V. At an overpotential of 0.4 V, the current density of PHI-Co dramatically dropped more than tenfold from 117.5 to 8.3 mA cm^{-2}. To exclude the influence of KSCN on PHI, the same poisoning test was carried out with pure PHI (Figure S9, Supporting Information), showing negligible differences of OER activity, so that the cobalt species are verified as active sites of PHI-Co. From XRD (Figure 1) and XPS Co 2p and O 1s measurements (Figure 2b and Figure S5, Supporting Information), no metallic cobalt or cobalt oxides can be detected in PHI-Co, indicating that the active sites in PHI-Co are the Co^{2+} ions within the PHI structure.

The stability of best-performing catalyst, PHI-Co-0.5, was measured under constant current densities of 10 mA cm^{-2}

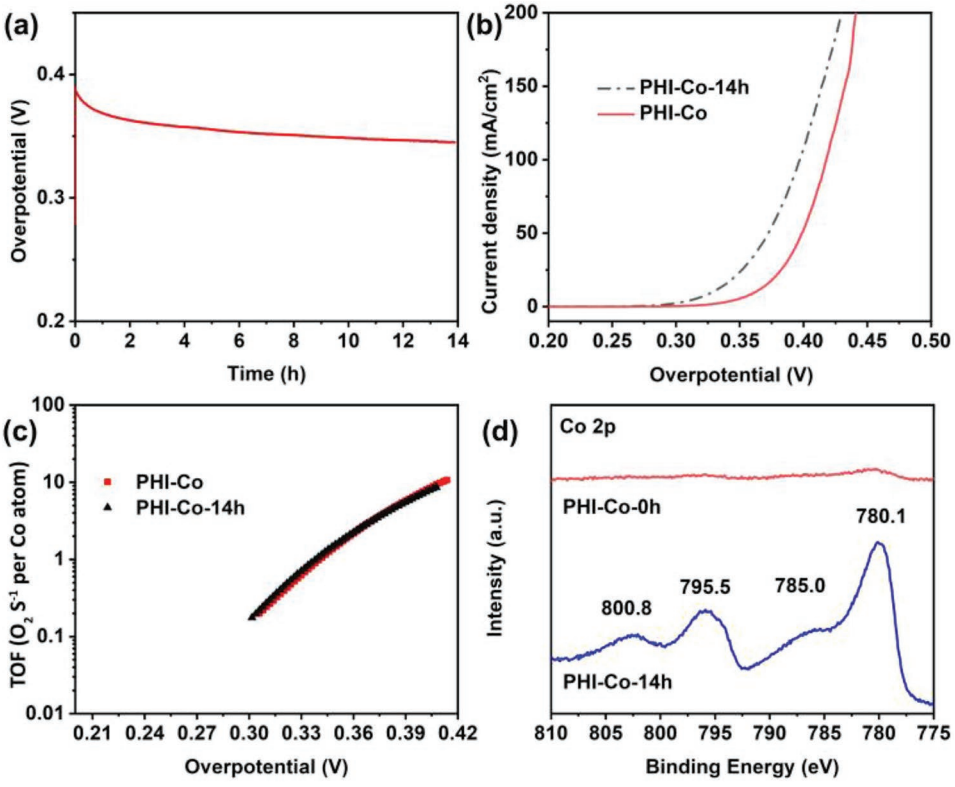

Figure 5. a) Stability test of PHI-Co-0.5 in 1 M KOH for ≈14 h. b) Polarization curves of PHI-Co before and after stability test. c) TOF to overpotential plots of PHI-Co before and after stability test. d) Co 2p XPS spectra of PHI-Co before and after ≈14 h of stability test.

for 5×10^5 s (≈14 h, **Figure 5**a). The OER polarization curves before and after the chronopotentiometric stability test are also presented in Figure 5b. Notably, during the chronopotentiometric stability test, the overpotential of PHI shows a continuous decrease by 0.04 V, which is also seen in the polarization curves of PHI-Co before and after the stability test (marked as PHI-Co and PHI-Co-14h). This gradually increased activity can also be observed in the cyclic stability test (Figure S10a, Supporting Information). To understand the activity change during the measurement, the TOF and Tafel slope before and after the stability test are given in Figure 5c and Figure S10b,c in the Supporting Information. Interestingly, despite the increased activity observed during the stability test, the activity per cobalt active sites and the reaction kinetics of the reaction barely changed. The chemical structure of PHI-Co before and after the stability test provides more insight to this phenomenon. XPS and IR spectra of the PHI-Co film on the electrode were recorded before and after the stability test (Figure 5d and Figures S11–S13, Supporting Information). The signal of Co 2p on the surface of the PHI-Co electrode has remarkably increased after the stability test while the oxidation state of Co stays the same (Figure 5d and Figure S11, Supporting Information), suggesting the cobalt ions slowly migrated from the bulk of PHI-Co to the surface. Still, no trace of cobalt oxides can be detected from the XPS O 1s spectra after the stability test (Figure S12, Supporting Information).[32] Also, no significant change is observed in the N 1s, C 1s spectra and IR spectra before and after stability test (Figure S13, Supporting Information), indicating that the basic structure of poly(heptazine) imide stays intact. Therefore, it can be concluded that the increased OER performance is due to the accumulation of the Co^{2+} on the surface.

In summary, PHI-Co was synthesized via a simple mixed salt melt method. Due to the enhanced conductivity and abundance, well-distributed Co–N_x catalytic active sites, this PHI-Co exhibits an excellent OER activity and stability, comparable to the state-of-the-art OER electrocatalysts under similar conditions. This work provides a novel approach to develop high-performance electrocatalysts with adjustable and highly dispersed metal–N_x sites by applying PHI as the supporting material.

Supporting Information

Supporting Information is available from the Wiley Online Library or from the author.

Acknowledgements

This work was funded by the Deutsche Forschungsgemeinschaft (DFG, German Research Foundation) under Germany's Excellence Strategy—EXC 2008/1–390540038. Gefördert durch die Deutsche Forschungsgemeinschaft (DFG) im Rahmen der Exzellenzstrategie des Bundes und der Länder—EXC 2008/1–390540038. Furthermore funding through the DFG project TH 1463/12-1 is acknowledged.

Conflict of Interest

The authors declare no conflict of interest.

Keywords

carbon nitride, electrocatalysis, M–N_x–C, oxygen evolution reaction, poly(heptazine imides)

Received: June 21, 2019
Revised: December 4, 2019
Published online: January 27, 2020

[1] S. Cobo, J. Heidkamp, P. A. Jacques, J. Fize, V. Fourmond, L. Guetaz, B. Jousselme, V. Ivanova, H. Dau, S. Palacin, M. Fontecave, V. Artero, *Nat. Mater.* **2012**, *11*, 802.
[2] X. Zhao, P. Pachfule, S. Li, T. Langenhahn, M. Ye, C. Schlesiger, S. Praetz, J. Schmidt, A. Thomas, *J. Am. Chem. Soc.* **2019**, *141*, 16.
[3] Y. Liao, Q. Chen, Y. Yang, B. Hou, M. Zhu, A. Thomas, H. Wang, *Small* **2018**, *14*, 1803232.
[4] C. C. L. McCrory, S. Jung, J. C. Peters, T. F. Jaramillo, *J. Am. Chem. Soc.* **2013**, *135*, 16977.
[5] Y. Liang, Y. Li, H. Wang, J. Zhou, J. Wang, T. Regier, H. Dai, *Nat. Mater.* **2011**, *10*, 780.
[6] X. Zhao, P. Pachfule, S. Li, J. R. J. Simke, J. Schmidt, A. Thomas, *Angew. Chem., Int. Ed.* **2018**, *57*, 8921.
[7] N. Danilovic, R. Subbaraman, K. C. Chang, S. H. Chang, Y. J. Kang, J. Snyder, A. P. Paulikas, D. Strmcnik, Y. T. Kim, D. Myers, *J. Phys. Chem. Lett.* **2014**, *5*, 2474.
[8] H. G. Sanchezcasalongue, M. L. Ng, S. Kaya, D. Friebel, H. Ogasawara, A. Nilsson, *Angew. Chem., Int. Ed.* **2014**, *53*, 7169.
[9] T. Reier, M. Oezaslan, P. Strasser, *ACS Catal.* **2012**, *2*, 1765.
[10] J. Kim, X. Yin, K. C. Tsao, S. Fang, H. Yang, *J. Am. Chem. Soc.* **2014**, *136*, 14646.
[11] I. C. Man, H. Y. Su, F. Calle-Vallejo, H. A. Hansen, J. I. Martínez, N. G. Inoglu, J. Kitchin, T. F. Jaramillo, J. K. Nørskov, J. Rossmeisl, *ChemCatChem* **2011**, *3*, 1159.
[12] C. Cheng, S. Li, Y. Xia, L. Ma, C. Nie, C. Roth, A. Thomas, R. Haag, *Adv. Mater.* **2018**, *30*, 1802669.
[13] P. Yin, T. Yao, Y. Wu, L. Zheng, Y. Lin, W. Liu, H. Ju, J. Zhu, X. Hong, Z. Deng, G. Zhou, S. Wei, Y. Li, *Angew. Chem., Int. Ed.* **2016**, *55*, 10800.
[14] W. Liu, L. Zhang, W. Yan, X. Liu, X. Yang, S. Miao, W. Wang, A. Wang, T. Zhang, *Chem. Sci.* **2016**, *7*, 5758.
[15] G. Wu, A. Santandreu, W. Kellogg, S. Gupta, O. Ogoke, H. Zhang, H. L. Wang, L. Dai, *Nano Energy* **2016**, *29*, 83.
[16] Y. Tang, R. Liu, S. Liu, B. Zheng, Y. Lu, R. Fu, D. Wu, M. Zhang, M. Rong, *Carbon* **2019**, *141*, 704.
[17] T. Schiros, D. Nordlund, L. Pálová, D. Prezzi, L. Zhao, K. S. Kim, U. Wurstbauer, C. Gutiérrez, D. Delongchamp, C. Jaye, *Nano Lett.* **2012**, *12*, 4025.
[18] X. Wang, K. Maeda, A. Thomas, K. Takanabe, G. Xin, J. M. Carlsson, K. Domen, M. Antonietti, *Nat. Mater.* **2009**, *8*, 76.
[19] A. Thomas, A. Fischer, F. Goettmann, M. Antonietti, J. O. Müller, R. Schlögl, J. M. Carlsson, *J. Mater. Chem.* **2008**, *18*, 4893.
[20] M. Y. Ye, Z. H. Zhao, Z. F. Hu, L. Q. Liu, H. M. Ji, Z. R. Shen, T. Y. Ma, *Angew. Chem., Int. Ed.* **2017**, *56*, 8407.
[21] M. M. Islam, R. D. Tentu, M. A. Ali, S. Basu, *ChemistrySelect* **2018**, *3*, 11241.
[22] A. Savateev, S. Pronkin, J. D. Epping, M. G. Willinger, C. Wolff, D. Neher, M. Antonietti, D. Dontsova, *ChemCatChem* **2017**, *9*, 167.
[23] Z. Chen, A. Savateev, S. Pronkin, V. Papaefthimiou, C. Wolff, M. G. Willinger, E. Willinger, D. Neher, M. Antonietti, D. Dontsova, *Adv. Mater.* **2017**, *29*, 1700555.
[24] Y. S. Jun, E. Z. Lee, X. C. Wang, W. H. Hong, G. D. Stucky, A. Thomas, *Adv. Funct. Mater.* **2013**, *23*, 3661.

[25] Y. S. Jun, W. H. Hong, M. Antonietti, A. Thomas, *Adv. Mater.* **2009**, *21*, 4270.
[26] M. J. Bojdys, J. O. Müller, M. Antonietti, A. Thomas, *Chem. – Eur. J.* **2008**, *14*, 8177.
[27] A. Savateev, S. Pronkin, M. G. Willinger, M. Antonietti, D. Dontsova, *Chem. – Asian J.* **2017**, *12*, 1517.
[28] D. Dontsova, S. Pronkin, M. Wehle, Z. Chen, C. Fettkenhauer, G. Clavel, M. Antonietti, *Chem. Mater.* **2015**, *27*, 5170.
[29] H. Schlomberg, J. Kröger, G. Savasci, M. W. Terban, S. Bette, I. Moudrakovski, V. Duppel, F. Podjaski, R. Siegel, J. Senker, R. E. Dinnebier, C. Ochsenfeld, B. V. Lotsch, *Chem. Mater.* **2019**, *31*, 7478.
[30] F. Podjaski, J. Kröger, B. V. Lotsch, *Adv. Mater.* **2018**, *30*, 1705477.
[31] X. K. Wang, J. W. Tian, D. D. Huang, Y. P. Wu, L. Q. Pan, D. S. Li, *J. Solid State Chem.* **2019**, *269*, 348.
[32] Z. Liao, Y. Wang, Q. Wang, Y. Cheng, Z. Xiang, *Appl. Catal., B* **2019**, *243*, 204.
[33] M. C. Biesinger, B. P. Payne, A. P. Grosvenor, L. W. Lau, A. R. Gerson, R. S. C. Smart, *Appl. Surf. Sci.* **2011**, *257*, 2717.
[34] A. Zambon, J. M. Mouesca, C. Gheorghiu, P. A. Bayle, J. Pécaut, M. Claeys-Bruno, L. Dubois, *Chem. Sci.* **2016**, *7*, 945.
[35] S. Li, C. Cheng, A. Sagaltchik, P. Pachfule, C. Zhao, A. Thomas, *Adv. Funct. Mater.* **2019**, *29*, 1970013.
[36] I. Monte-Pérez, S. Kundu, A. Chandra, K. E. Craigo, P. Chernev, U. Kuhlmann, N. Lehnert, *J. Am. Chem. Soc.* **2017**, *139*, 15033.
[37] W. Wang, D. D. Babu, Y. Huang, J. Lv, Y. Wang, M. Wu, *Int. J. Hydrogen Energy* **2018**, *43*, 10351.
[38] H. Jia, Y. Yao, J. Zhao, Y. Gao, Z. Luo, P. Du, *J. Mater. Chem. A* **2018**, *6*, 1188.
[39] J. Hou, Y. Sun, Z. Li, B. Zhang, S. Cao, Y. Wu, Z. Gao, L. Sun, *Adv. Funct. Mater.* **2018**, *28*, 1803278.
[40] M. Shakeel, M. Arif, G. Yasin, B. Li, H. D. Khan, *Appl. Catal., B* **2019**, *242*, 485.
[41] Y. Xu, B. Li, S. Zheng, P. Wu, J. Zhan, H. Xue, Q. Xu, H. Pang, *J. Mater. Chem. A* **2018**, *6*, 22070.
[42] X. F. Lu, P. Q. Liao, J. W. Wang, J. X. Wu, X. W. Chen, C. T. He, J. P. Zhang, G. R. Li, X. M. Chen, *J. Am. Chem. Soc.* **2016**, *138*, 8336.
[43] S. Zhao, Y. Wang, J. Dong, C. T. He, H. Yin, P. An, K. Zhao, X. Zhang, C. Gao, L. Zhang, J. Lv, J. Wang, J. Zhang, A. M. Khattak, N. A. Khan, Z. Wei, J. Zhang, S. Liu, H. Zhao, Z. Tang, *Nat. Energy* **2016**, *1*, 16184.
[44] O. V. Magdysyuk, F. Adams, H.-P. Liermann, I. Spanopoulos, P. N. Trikalitis, M. Hirscher, R. E. Morris, M. J. Duncan, L. J. McCormick, R. E. Dinnebier, *Phys. Chem. Chem. Phys.* **2014**, *16*, 23908.
[45] J. Cao, C. Lei, J. Yang, X. Cheng, Z. Li, B. Yang, X. Zhang, L. Lei, Y. Hou, K. Ostrikov, *J. Mater. Chem. A* **2018**, *6*, 18877.
[46] X. L. Wang, L. Z. Dong, M. Qiao, Y. J. Tang, J. Liu, Y. Li, S. L. Li, J. X. Su, Y. Q. Lan, *Angew. Chem., Int. Ed.* **2018**, *57*, 9660.
[47] N. T. Suen, S. F. Hung, Q. Quan, N. Zhang, Y. J. Xu, H. M. Chen, *Chem. Soc. Rev.* **2017**, *46*, 337.
[48] S. Anantharaj, S. R. Ede, K. Sakthikumar, K. Karthick, S. Mishra, S. Kundu, *ACS Catal.* **2016**, *6*, 8069.
[49] H. W. Liang, S. Brüller, R. Dong, J. Zhang, X. Feng, K. Müllen, *Nat. Commun.* **2015**, *59*, 149.